ADVANCED MATERIALS INTERFACES
www.advmatinterfaces.de

Intermediate Structures of Nucleation and Growth during Solidification of CuO Constrained by Graphene

Mengke Ge, Wenjuan Yuan, Lingling Zhou, Ziliang Deng, Min Hu, Xiang Li, Jia He, Wei Xi,* and Jun Luo*

Important solid-state information regarding solidification remains unknown, such as the intermediate structure before nucleation and precipitation pathways for each component in multicomponent materials during crystal growth. Herein, a unique intermediate structure with unequal lattice structure (the main performance is the curved lattice fringes and the unequal interplanar spacing) is observed in situ at the atomic level before CuO nucleation. The results of experiments and molecular dynamics simulations indicate that the formation of this intermediate may be due to the irregular agglomeration of Cu and O atoms. During growth, Cu–Cu layers repeatedly form at the solid–liquid interface as an intermediate state, then oxidizes, and finally forms a perfect CuO crystal. These results help to reveal the mystery of nucleation nanomaterials, especially the multicomponent materials, and elucidate microscopic crystal growth mechanisms during multicomponent materials solidification.

Solidification and melting are key issues in solid-state physics[1,2] and materials science,[3–5] but knowledge of their mechanisms is lacking. Thus, it is important to establish a basic understanding of these elusive process mechanisms. Theoretically, the crystallization process during solidification consists of two parts: nucleation and crystal growth. In particular, particles nucleate at one site and grow outward through atomic migration and deposition.[6]

However, the classical nucleation theory has certain limitations. For the investigation of crystallization, many researchers have reported that multistep pathways involve prenucleation clusters or amorphous intermediates before the formation of thermodynamically stable nuclei.[7–14] Meanwhile, prenucleation during solidification has not been studied owing to the lack of effective techniques. Thus, the existence of intermediate structures and the manner of transformation into nuclei remain unclear and require atomic-scale investigation.

Some researchers have studied the crystal growth process during solidification of a Bi and colloid model.[15–21] For single-component materials, such as Bi, the mechanism of crystal growth is relatively clear. The atoms interact to form Bi—Bi bonds with the same arrangement as the Bi crystal to form a periodic Bi crystal structure (crystallization along the $[1\bar{1}0]$ direction).[21] However, for the crystal growth processes of multicomponent materials (such as binary materials), the manner of precipitation for each component remains unknown; for example, it is unclear whether sequential precipitation or simultaneous coordinated precipitation occurs during crystal growth. Answering this question is challenging because of the complexity of the growth process and technical limitations.

Studying intermediate structures during the prenucleation and precipitation of each component in multicomponent materials is important for understanding solidification theory. In this study, nucleation and crystal growth processes during the solidification of CuO nanoparticles (NPs) constrained by graphene were observed on the atomic scale by in situ transmission electron microscopy (TEM). The results show that the intermediate structure of the nucleus is different from the crystal, amorphous, and quasicrystal structures. The crystal grows more quickly in the [002] direction than in the $[11\bar{1}]$ orientations; therefore, two layers of Cu were observed at the solid–liquid interface along the [002] orientation. Ultimately, a perfect CuO crystal formed. These observations provide intuitive evidence for understanding the microscopic solidification mechanisms of this system.

In this experiment, Cu nanoparticles were prepared by mechanical ball milling and high temperature reduction. First, pure Cu powder (5 g, 99.99%, 100 mesh) was treated by ball milling in 100 mL $CuCl_2$ solution with $[Cl^-] = 0.75 \times 10^{-2}$ mol L^{-1}. The rotating speed of ball milling was 400 rpm and the duration was 25 h. The size of the mill balls was 15 mm and the ballto-powder weight ratio was 20:1. The as-milled product

M. Ge, Dr. W. Yuan, Z. Deng, M. Hu, X. Li, Dr. J. He,
Dr. W. Xi, Prof. J. Luo
Center for Electron Microscopy and Tianjin Key Laboratory
of Advanced Functional Porous Materials
Institute for New Energy Materials & Low-Carbon Technologies
School of Materials Science and Engineering
Tianjin University of Technology
Tianjin 300384, China
E-mail: hejia@tjut.edu.cn; xiwei@email.tjut.edu.cn
Dr. L. Zhou
State Key Laboratory of Nonlinear Mechanics
Institute of Mechanics
Chinese Academy of Sciences
Beijing 100190, China
The ORCID identification number(s) for the author(s) of this article can be found under https://doi.org/10.1002/admi.201902047.

DOI: 10.1002/admi.201902047

was rinsed with distilled water and then dried in vacuum at 40 °C for 2 h. Finally, Cu NPs were obtained by reducing the resulting products at 400 °C for 15 min under ammonia. The prepared Cu NPs were dispersed with ethanol and dropped on a heating chip (Wildfire S5, DENSsolutions, Netherlands) before in situ TEM experiments. The heating range was 23–1100 °C, the heating rate was 30 °C min^{-1}, and the temperature error was <5%. The solidification of CuO NPs was observed by using high-resolution field-emission TEM (Talos F200X, Thermo Fisher Scientific) at an accelerating voltage of 200 kV, and video and images were recorded using a charge-coupled device camera.

Molecular dynamics (MD) simulations were carried out through the large-scale atomic/molecular massively parallel simulator (LAMMPS)[22] with a time step of 0.5 fs in the NVT ensemble (an ensemble with the number of particles N, the volume V and the absolute temperature T in the system) at 350 K. In the geometry optimizations and MD simulations, the atoms in the bottom 5 Å were kept fixed. During the simulation, Cu and O atoms were deposited every 5 ps at a distance of >10 Å above the solid–vacuum interface. The MD simulation parameters for nucleation[23] and growth[24] were taken from previous studies. First-principles calculations were performed using the DMol3 code,[25] for which the Perdew–Burke–Ernzerhof exchange-correlation functional was employed within the generalized gradient approximation.[26] Double numerical plus polarization was chosen as the basis set for other elements. During geometry optimizations, the K-points were set as $5 \times 5 \times 1$.

The prepared partially oxidized Cu NPs ranged in size from 10 to 150 nm (**Figure 1**a). At 23 °C, the Cu NPs were polyhedrons with good crystallinity (Figure 1b), and amorphous carbon covered the surface. Owing to the small size of the NPs, the melting point was reduced below that of the bulk, meaning they melted completely at 1064 °C (Figure 1c). Low magnification morphology diagrams of particles at different temperatures are shown in Figure S1 in the Supporting Information. The surface of the molten droplets was coated with graphene. At such high temperatures, amorphous carbon was considered to convert to graphene.[27]

During the heat preservation process at 1064 °C, the shape of the droplet changed, as shown in **Figure 2**a. The nucleation pathways were strongly influenced by the adhesion of the surfaces of the CuO NPs with the carbon capping shell. This can be attributed the modification of the surface free energy by the carbon-shell substrate.[28–31] Notably, facets formed at the surface, which are a precursor to nucleation.[21] After 0.1 s, a hat-shaped metastable nucleus intermediate structure formed at the lower corner of the droplet (white dotted line) as shown in Figure 2b. Magnifying this intermediate structure, as shown in Figure 2c, shows that it has a twisted discontinuous layered structure with interlayer distances ranging from 0.21 to 0.24 nm. This configuration is different from the crystal (periodic long-range order), amorphous (short-range order, long-range disorder), and quasicrystal (ordered without translational symmetry) structures (Figure 2c). Previous reports have shown that amorphous intermediate structures form in monolithic materials.[7] The observed difference may be due to the characteristics of the binary materials.

The prenucleation process was also explored via MD simulations by randomly depositing Cu and O atoms on a graphene surface. As shown in Figure 2d–f and Movie S2 in the Supporting Information, the Cu atoms initially tend to agglomerate on the substrate, and O atoms are relatively dispersed (Figure 2d). Subsequently, the increasing number of O atoms spread into the Cu cluster (Figure 2e), ultimately forming a twisted discontinuous layered structure (Figure 2f). This finding may indicate that the solidification process of multicomponent materials is driven by preferential segregation of a certain component, following which the other components refuse to form an ordered structure.

With increasing time, an ordered crystal formed and grew toward the inside of the droplet, as shown in **Figure 3**a–e. Additionally, the fast Fourier transform of particles at different times during solidification were shown in Figure S2 in the Supporting Information. The increase in thickness of the crystal plane was analyzed by recording the position of the solid–liquid interface at different times (Figure 3e). The growth rate in the [002] orientation was significantly higher than that in the [11$\bar{1}$] direction until the final-order CuO particle formed. First-principles calculations revealed that the surface energy of the {002} plane is higher than that of the {11$\bar{1}$} plane (Figure S3, Supporting Information). This result is similar to the previously observed growth pathways of octahedral Pt_3Ni NPs under CO,[32] wherein the layer-by-layer growth of the {111} facet was inhibited by CO.

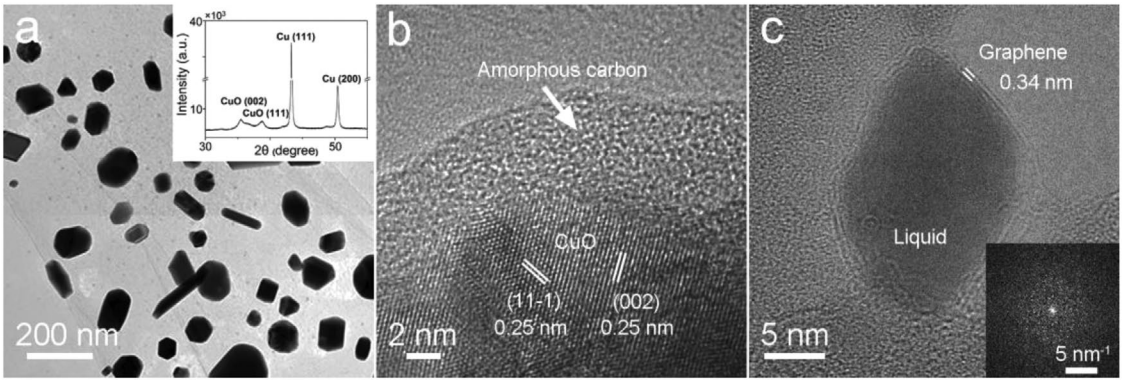

Figure 1. Characterizations of partially oxidized Cu NPs at different temperatures. a) Low-magnification TEM image of NPs at 23 °C. Inset: XRD pattern. b) TEM image of one CuO NP. c) Droplet of a partially oxidized Cu NP after melting at 1064 °C. Inset: corresponding diffraction pattern.

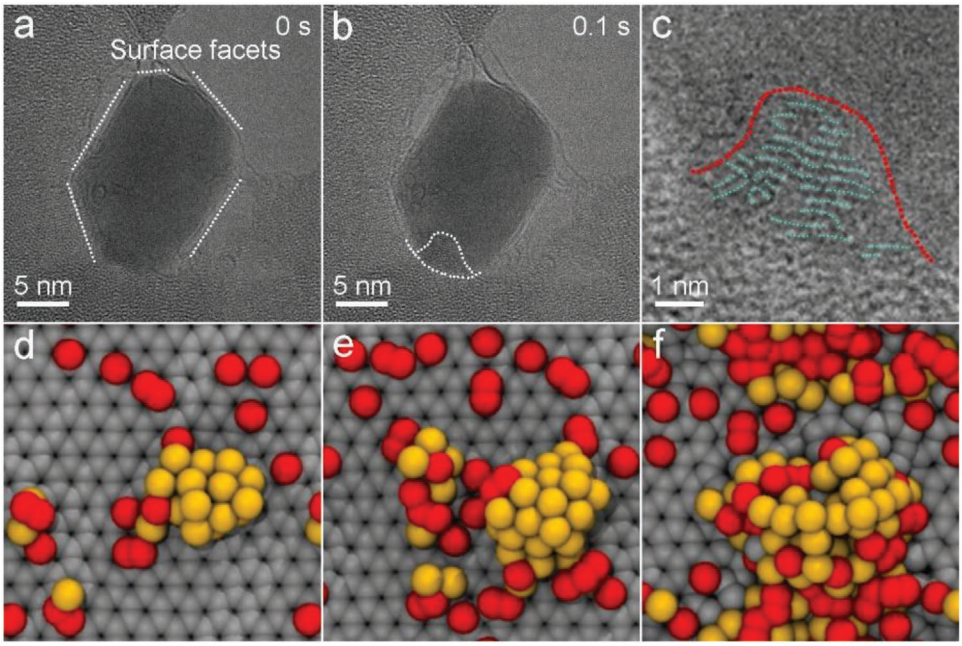

Figure 2. Nucleation process of CuO droplets during solidification. a) Formation of surface facets before nucleation. b) HRTEM image of the intermediate structure of the nucleus. c) Enlarged view of the intermediate structure of the nucleus shown in (b). The red dotted line represents the outline, and the cyan dotted lines represent layers of the intermediate structure. d–f) Snapshots of MD-simulated Cu and O atom deposition on graphene at 100, 200, and 400 ps. Yellow balls: Cu atoms; red balls: O atoms; gray balls: C atoms. (a–c) are taken from Movie S1 in the Supporting Information. (d–f) are taken from Movie S2 in the Supporting Information.

It is well known that during rapid solidification processes, defects form easily inside the crystal. Before 0.5 s, the growth rate of the crystal was high, as shown in Figure 3e, resulting in a stacking fault inside the crystal (Figure 3a). After crystal growth was completed, the left part of the particle translated upward (Figure 3c), and the stacking fault disappeared, resulting in a perfect crystal (Figure 3e).

At the prenucleation stage of solidification, the Cu and O atoms are not synergistically precipitated; this same phenomenon appears during the crystal growth process. Occasionally, the interplanar spacing of the topmost layer at the solid–liquid interface is 0.21 nm along the [002] orientation (Figure 3f; Figure S4, Supporting Information). This spacing is smaller than the internal interplanar spacing (0.25 nm) and is the same as that for Cu (111). This finding may indicate that Cu layers form at the solid–liquid interface during the solidification process. Subsequently, Cu combines with O to form CuO crystals owing to O diffusion (Figure S5, Supporting Information). The above analysis was further supported by the MD simulations. The structures of the three different low-index crystal facets—(111), (110), and (100)—of Cu flake epitaxial growth on a CuO substrate were calculated, and the corresponding total energy evolution profiles are shown in Figure 3g. In the initial stage of the simulation (0–10 ps), the energy of the Cu (111) layer was significantly lower than that of the other two crystal facets, indicating that the (111) facet is the most favorable. Notably, the configurations of the (110) and (100) facets gradually evolved into the (111) facet, whereas the structure of the (111) facet did not obviously fluctuate during the simulation (Movies S3–S5, Supporting Information). Thus, in the later stage of the simulation, the energy difference between the three crystal facets decreases owing to structural convergence. This theoretical calculation demonstrates that the Cu (111) layer is the most favorable conformation for epitaxial growth on the CuO (002) surface, which is in accordance with the TEM observations.

In previous studies, solidification was considered a process of mutation with an extremely short time span,[33] making it highly difficult to observe. In our work, because the surface of the droplet was constrained by graphene, the solidification time was extremely prolonged, which enabled easy and clear monitoring of the nucleation and crystal growth. This method can be applied to observe the solidification process of other droplets, as evidenced by MD calculations regarding melting.[34] The wide applicability of this method will be of great significance to the development of solidification theory.

The solidification process of CuO NPs constrained by graphene was observed using in situ high-resolution TEM (HRTEM). The experimental and theoretical results show that the intermediate structure before nucleation is different from the crystal, amorphous, and quasicrystal structures. In the prenucleation stage, Cu atoms tend to agglomerate on the substrate, and the increased number of surrounding O atoms diffuses into the Cu cluster to form a twisted discontinuous layered structure. During the crystal growth process, the [002] orientation grows faster than the [11$\bar{1}$] orientation because of the higher energy of the (002) plane. Furthermore, at the solid–liquid interface, an intermediate growth structure of two Cu layers can sometimes form. Subsequently, O diffuses into this structure and combines with Cu atoms to form CuO crystals. These observations of the evolution of solidification dynamics

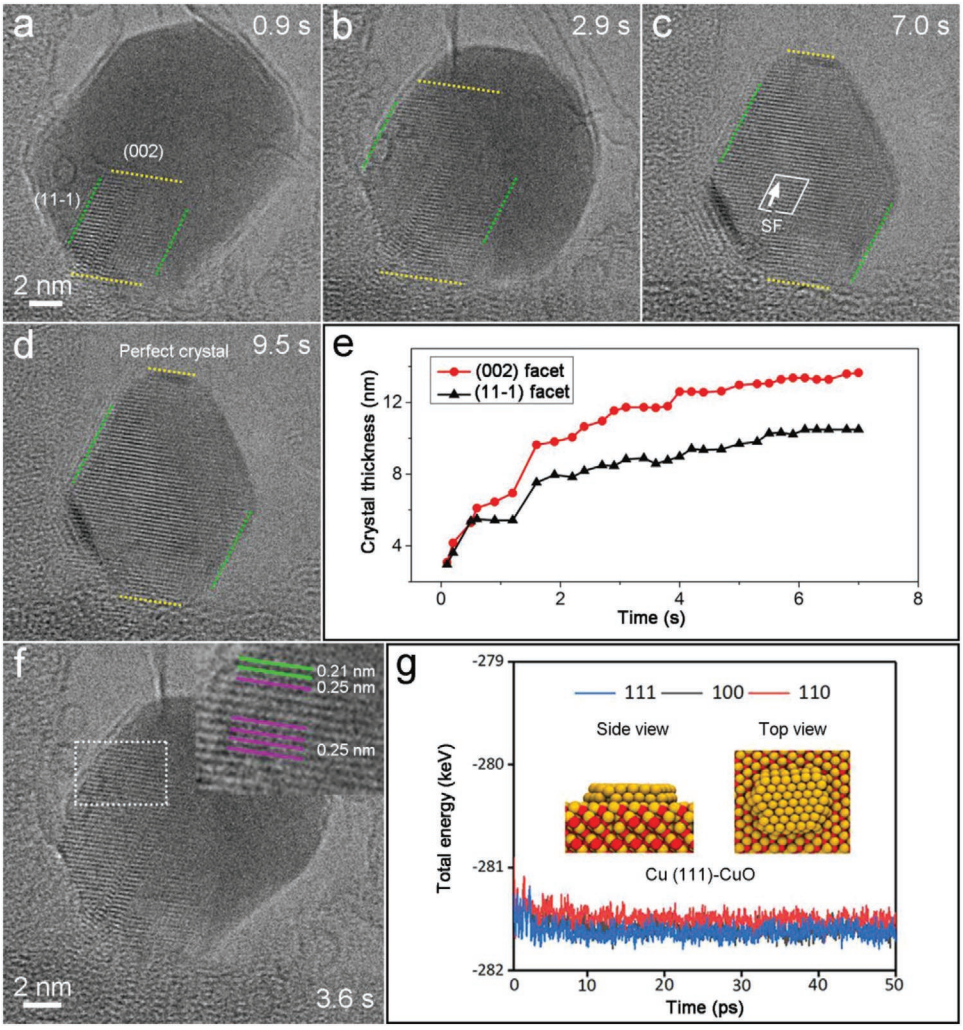

Figure 3. Crystal growth of CuO NPs. a–d) TEM images of CuO crystal at different times. The yellow and green dotted lines correspond to the (002) and (11-1) facets, respectively, and the images have the same scale bar. The SF in (c) represents stacking faults formed during the growth of CuO NPs, with the solid white line representing its Burgers loop and the arrow representing its slip direction to make it invisible. e) Variation in crystal thickness of (002) and (11-1) orientations versus time. f) Growth intermediate structure of CuO NP. f) HRTEM image of the intermediate structure during CuO crystal growth. The inset shows an enlarged image of the area within the white box. g) Time evolution of the total energy of Cu (111), (110), and (100) flakes grown on a CuO (002) substrate.

provide fundamental evidence for understanding the nucleation and growth mechanisms. Moreover, the method used in this study will provide new directions for solidification theory research.

Supporting Information

Supporting Information is available from the Wiley Online Library or from the author.

Acknowledgements

M.G., W.Y., and L.Z. contributed equally to this work. This work was financially supported by the National Key R&D Program of China (2017YFA0700104), the National Natural Science Foundation of China (51701143, 21603161, 51971157, and 51761165012), the Tianjin Municipal Science and Technology Commission (18JCYBJC86900), Tianjin Science Fund for Distinguished Young Scholars, and National Program for Thousand Young Talents of China, and Wuxi Research Institute of Applied Technologies, Tsinghua University.

Conflict of Interest

The authors declare no conflict of interest.

Keywords

CuO, intermediate structures, nucleation, solidification

Received: December 4, 2019
Revised: January 18, 2020
Published online: February 17, 2020

[1] A. M. Alsayed, M. F. Islam, J. Zhang, P. J. Collings, A. G. Yodh, *Science* **2005**, *309*, 1207.
[2] J. G. Dash, A. W. Rempel, J. S. Wettlaufer, *Rev. Mod. Phys.* **2006**, *78*, 695.
[3] M. Liu, Y. Ma, H. Wu, R. Y. Wang, *ACS Nano* **2015**, *9*, 1341.
[4] P. Krogstrup, *Nat. Mater.* **2015**, *14*, 757.
[5] H. Wang, J.-T. Wang, Z.-X. Cao, W.-J. Zhang, C.-S. Lee, S.-T. Lee, X.-H. Zhang, *Nat. Commun.* **2015**, *6*, 6412.
[6] D. Turnbull, *J. Appl. Phys.* **1950**, *21*, 1022.
[7] L. Fei, X. Gan, S. M. Ng, H. Wang, M. Xu, W. Lu, Y. Zhou, C. W. Leung, C.-L. Mak, Y. Wang, *ACS Nano* **2019**, *13*, 681.
[8] Y. Li, L. Zang, D. L. Jacobs, J. Zhao, X. Yue, C. Wang, *Nat. Commun.* **2017**, *8*, 14462.
[9] N. D. Loh, S. Sen, M. Bosman, S. F. Tan, J. Zhong, C. A. Nijhuis, P. Král, P. Matsudaira, U. Mirsaidov, *Nat. Chem.* **2017**, *9*, 77.
[10] J. Lee, J. Yang, S. G. Kwon, T. Hyeon, *Nat. Rev. Mater.* **2016**, *1*, 16034.
[11] J. J. De Yoreo, P. U. P. A. Gilbert, N. A. J. M. Sommerdijk, R. L. Penn, S. Whitelam, D. Joester, H. Zhang, J. D. Rimer, A. Navrotsky, J. F. Banfield, A. F. Wallace, F. M. Michel, F. C. Meldrum, H. Cölfen, P. M. Dove, *Science* **2015**, *349*, aaa6760.
[12] N. T. K. Thanh, N. Maclean, S. Mahiddine, *Chem. Rev.* **2014**, *114*, 7610.
[13] W. J. E. M. Habraken, J. Tao, L. J. Brylka, H. Friedrich, L. Bertinetti, A. S. Schenk, A. Verch, V. Dmitrovic, P. H. H. Bomans, P. M. Frederik, J. Laven, P. van der Schoot, B. Aichmayer, G. de With, J. J. De Yoreo, N. A. J. M. Sommerdijk, *Nat. Commun.* **2013**, *4*, 1507.
[14] D. Gebauer, H. Cölfen, *Nano Today* **2011**, *6*, 564.
[15] M. H. Nielsen, S. Aloni, J. J. De Yoreo, *Science* **2014**, *345*, 1158.
[16] J. M. Yuk, J. Park, P. Ercius, K. Kim, D. J. Hellebusch, M. F. Crommie, J. Y. Lee, A. Zettl, A. P. Alivisatos, *Science* **2012**, *336*, 61.
[17] J. Li, Z. Wang, F. L. Deepak, *ACS Nano* **2017**, *11*, 5590.
[18] J. Li, Z. Wang, F. L. Deepak, *J. Phys. Chem. Lett.* **2018**, *9*, 961.
[19] Y. Li, B. R. Bunes, L. Zang, J. Zhao, Y. Li, Y. Zhu, C. Wang, *ACS Nano* **2016**, *10*, 2386.
[20] C. Luo, K. Yu, X. Wu, L. Sun, *Phys. Status Solidi B* **2019**, *256*, 1800442.
[21] Y. Li, M. Huang, L. Zang, D. L. Jacobs, J. Zhao, Y. Zhu, C. Wang, *Cryst. Growth Des.* **2018**, *18*, 5808.
[22] P. W. Sutter, E. A. Sutter, *Nat. Mater.* **2007**, *6*, 363.
[23] S. Plimpton, *J. Comput. Phys.* **1995**, *117*, 1.
[24] T. Liang, T.-R. Shan, Y.-T. Cheng, B. D. Devine, M. Noordhoek, Y. Li, Z. Lu, S. R. Phillpot, S. B. Sinnott, *Mater. Sci. Eng., R* **2013**, *74*, 255.
[25] A. C. T. van Duin, V. S. Bryantsev, M. S. Diallo, W. A. Goddard, O. Rahaman, D. J. Doren, D. Raymand, K. Hermansson, *J. Phys. Chem. A* **2010**, *114*, 9507.
[26] B. Delley, *J. Chem. Phys.* **2000**, *113*, 7756.
[27] F. Börrnert, S. M. Avdoshenko, A. Bachmatiuk, I. Ibrahim, B. Büchner, G. Cuniberti, M. H. Rümmeli, *Adv. Mater.* **2012**, *24*, 5630.
[28] Y. Ding, F. Fan, Z. Tian, Z. L. Wang, *Small* **2009**, *5*, 2812.
[29] J.-G. Lee, J. Lee, T. Tanaka, H. Mori, *Phys. Rev. Lett.* **2006**, *96*, 075504.
[30] M. A. Asoro, D. Kovar, P. J. Ferreira, *ACS Nano* **2013**, *7*, 7844.
[31] J. J. Li, Z. C. Wang, Y. P. Li, F. L. Deepak, *Adv. Sci.* **2019**, *6*, 1802131.
[32] J. P. Perdew, K. Burke, M. Ernzerhof, *Phys. Rev. Lett.* **1996**, *77*, 3865.
[33] X. Shen, C. Zhang, S. Zhang, S. Dai, G. Zhang, M. Ge, Y. Pan, S. M. Sharkey, G. W. Graham, A. Hunt, I. Waluyo, J. T. Miller, X. Pan, Z. Peng, *Nat. Commun.* **2018**, *9*, 4485.
[34] C. Chen, Z. Hu, Y. Li, L. Liu, H. Mori, Z. Wang, *Sci. Rep.* **2016**, *6*, 19545.

